

# Jitter Radiation In Gamma Ray Bursts and their afterglows: Emission and Self Absorption

Jared C. Workman<sup>1</sup>, Brian J. Morsony<sup>1</sup>, Davide Lazzati<sup>1</sup> and Mikhail V. Medvedev<sup>2</sup>

<sup>1</sup> JILA, University of Colorado, 440 UCB, Boulder, CO 80309-0440, USA

<sup>2</sup> Department of Physics and Astronomy, University of Kansas, Lawrence, KS 66045

7 February 2020

## ABSTRACT

Relativistic electrons moving into a highly tangled magnetic field emit jitter radiation. We present a detailed computation of the jitter radiation spectrum for electrons inside Weibel shock generated magnetic fields, including self-absorption. We apply our results to the case of the prompt and afterglow emission of gamma-ray bursts. We show that jitter emission can reproduce most of the observed features with some important differences with respect to standard synchrotron, especially between the self-absorption and the peak frequency. We discuss the similarities and differences between jitter and synchrotron and discuss experiments that can disentangle the two mechanisms.

**Key words:** gamma rays: bursts — magnetic fields — radiation mechanisms: non-thermal

## 1 INTRODUCTION

The external shock model (Meszaros & Rees 1997; Piran 1999) has been very successful in the explanation of afterglow radiation in gamma-ray bursts. In this model afterglow photons are produced by converting some of the internal energy of the burst blastwave into radiation. The radiation mechanism is supposed to be standard synchrotron produced by a population of relativistic electrons gyrating around a high intensity magnetic field. Synchrotron radiation is able to reproduce the spectra of some observed GRB afterglows (Wijers et al. 1999; Panaitescu & Kumar 2001), the temporal decays, their duration and the small level of linear polarization (Covino et al. 1999; Lazzati et al. 2004).

How the magnetic field is produced is however a matter of open debate. Compression of the interstellar magnetic field is not enough to explain the observed frequencies, and a strong magnetic field linked to the central object powering the explosion (e.g. the magnetic field of a neutron star) would decay too rapidly with radius. In the standard external shock model, it is assumed that a quasi equipartition magnetic field is generated by the shock and permeates the shocked interstellar medium (ISM) region without decaying. The fraction of energy given to the magnetic field is usually defined through  $B^2 = 8\pi\epsilon_B\rho$  where  $\rho$  is the energy density of the post-shock material. Synchrotron interpretation of prompt GRB spectra has however been unable to explain a sizable fraction of the spectra that display low-energy slopes steeper than  $nu^{1/3}$ , i.e., harder than what is allowed by synchrotron (Crider et al. 1997; Preece et al. 1998; Ghisellini et al. 2000).

Particle in cell (PIC) simulations of collisionless shocks

have demonstrated that the Weibel instability can produce magnetic fields at almost equipartition ( $\epsilon_B \sim 0.1$ , Silva et al. 2003; Fredriksen et al. 2004). Whether these fields can avoid dissipation and survive beyond the few plasma skin depths that current simulations can compute is a matter of open debate. (Gruzinov 2001; Medvedev et al. 2005). What is certain is that the field created by the Weibel instability has a very short coherence length, so that classical synchrotron formulae cannot be generally applied. Medvedev & Loeb (1999; see also Medvedev 2006; Fleishman 2006) derived the single electron spectral properties of radiation in the limit of a magnetic field with a very small coherence length: jitter radiation. The theory was applied to the prompt emission of gamma-ray bursts (GRBs) and was shown to be able to reproduce some characteristic features, such as the steep low-energy spectrum and the sharpness of the spectral break. Recently, jitter radiation model has been extended to the self-absorption regime (Medvedev, et al. 2007) and applied to GRB afterglows. The analytical spectra and lightcurves have been evaluated.

In this paper we review and refine the jitter theory including self-absorption, numerically implement it in our radiation code and apply it for the optical-UV range for the prompt emission. We also compare properties and spectral characteristics of jitter and synchrotron radiation models in the afterglow regime. We show that jitter radiation is a viable framework to interpret prompt and afterglow observations. We discuss the observational implications of this novel radiation mechanism and discuss some observational tests to compare synchrotron and jitter radiation in GRBs.

The paper is organized as follows: in § 2 we compute

the emissivity of jitter radiation and the absorption coefficient, in § 3 we apply our result to some cases relevant for GRB prompt and afterglow emission. We conclude in § 4 by discussing some implications for GRB observations.

## 2 SPECTRUM PRODUCED BY JITTER RADIATION

This section will lay the analytical framework by which to model the specific intensity  $I_\omega$  due to jitter radiation produced by Weibel generated magnetic fields. The first section deals with the specific nature of the magnetic field produced by the Weibel instability and used in our calculations. The second section discusses the mathematical formulation used to calculate the emission coefficient  $j_\omega$ , which describes the angle-averaged power per unit frequency added to the radiation field by electrons emitting jitter radiation. Finally, the third section describes how to obtain the absorption coefficient  $\alpha_\omega$ , which describes how jitter radiation self attenuates.

As a first step we have chosen to solve for the absorption and emission coefficients in the comoving frame. Although we calculate the comoving quantities, it is straightforward to transform to the observer frame by recalling that  $\alpha_\omega\omega$  and  $\frac{j_\omega}{\omega^2}$  are both Lorentz invariants with  $\omega = \omega'\gamma_b(1 + \frac{v}{c}\cos\theta')$  where  $\gamma_b$  and  $v$  refer to the bulk velocity of the object and not the Lorentz factors of the individual emitting electrons and  $\cos\theta'$  is defined by the angle between a photons path and the co-moving volume's direction. This algebraic transformation allows us to recast the equation for the observed intensity as a function of comoving quantities. Proceeding in this manner greatly simplifies the analytics and allows us to solve for the observed specific intensity by using numerically computed, comoving quantities.

### 2.1 Magnetic Fields In Gamma Ray Bursts

The standard model for emission from both the prompt burst in GRBs and the afterglow has relied mainly on the assumption that the radiative mechanism is synchrotron (Zhang & Meszaros 2004; Granot et al. 1999ab). While the assumption of synchrotron is reasonable for some of the observed prompt bursts due to strong magnetic field progenitors, it is unlikely that it is dominant in afterglow emission. Parameterizing the strength of the magnetic field by  $\epsilon_B$ , which is the ratio of the magnetic field energy density to the thermal energy density leads to values of  $\epsilon_B$  (from observations and simulations) ranging from  $10^{-1}$  to  $10^{-5}$  (Medvedev & Loeb 1999). If one assumes a strong field due to the source star of order  $10^{16}G$  and calculates the strength of this field due to simple volume expansion at a radius of  $10^{16}$  cm (approximately where afterglow radiation is emitted) it is easy to show ( $B \propto V^{-2/3}$ ) that the strength of the field is  $\sim 10^{-2}G$  corresponding to an  $\epsilon_B \sim 10^{-7}$  which is much too low to account for the actual observational and simulation results. Additionally, compressional generation of magnetic fields, which is  $\propto \gamma B_{ISM}$  is too weak to generate sufficiently strong fields at the afterglow shock front and results in values of  $\epsilon_B \sim 10^{-11}$  (Medvedev & Loeb 1999). With no new mechanism available to produce fields it is unlikely

that synchrotron can be the mechanism by which afterglow radiation is produced.

One very promising candidate for the origin of the magnetic field which results in afterglow emission comes from a relativistic version of the well known two-stream Weibel instability in a plasma. In the rest frame of a relativistic shock, the Weibel instability amplifies any existing magnetic field perturbations by growing current filaments out of instreaming electrons. The amplification of the current filaments is fed by the kinetic energy of the inflowing material (The ISM in the case of GRBs) and does not saturate until all of the energy in the particle distribution function's anisotropy is converted to magnetic field energy. Medvedev & Loeb (1999) have shown that the field is generated in the plane of the shock and has a coherence length of order the relativistic skin depth of the shock. Further numerical studies (Nishikawa et al. 2003; Silva et al. 2003; Fredriksen et al. 2004) have confirmed the existence and growth of this instability. For a detailed discussion of the Weibel instability see Medvedev & Loeb (1999). The major factor which makes magnetic fields generated via the Weibel instability unique is that the correlation length of the fields is less than a Larmor Radius and, as a result, the radiation generated by electrons in Weibel fields is very different than that generated by uniform large scale fields which result in Synchrotron radiation. Additionally, the field is generated in the plane of the shock and is then transported downstream as the shock propagates into the ISM. This continual generation of field is an attractive solution to the problem of how field is either generated or carried far enough downstream to produce the radiation observed in afterglows.

In this paper we adopt the model used by Medvedev (2006) to describe the magnetic field. The correlation tensor for the field is then given by

$$K_{\alpha\beta}(\mathbf{k}) = 4\pi C(\delta_{\alpha\beta} - n_\alpha n_\beta)f_z(k_\parallel)f_{xy}(k_\perp). \quad (1)$$

This form assumes that the field in the plane of the shock and the field in the direction of propagation can be factored from each other where  $f_{xy}(k_\perp) = (k_x^2 + k_y^2)^{1/2}$  describes the field in the plane of the shock,  $f_z(k_\parallel) = k_z$  describes the field in the direction of the shocks propagation, and  $C$  is a normalization constant. The functions used to describe the field are also taken from Medvedev (2006) in order to facilitate a direct comparison with the results therein and are given by

$$f_z(k_\parallel) = \frac{k_\parallel^{2\alpha_1}}{(\kappa_\parallel^2 + k_\parallel^2)^{\beta_1}}, \quad (2)$$

and

$$f_{xy}(k_\perp) = \frac{k_\perp^{2\alpha_2}}{(\kappa_\perp^2 + k_\perp^2)^{\beta_2}} \quad (3)$$

where  $\alpha_{1,2}$ ,  $\beta_{1,2}$ , and  $\kappa_{\perp,\parallel}$  are parameters used to fit the spectrum to numerical results. In this paper we have chosen  $\alpha_1 = \alpha_2$ ,  $\beta_1 = \beta_2$ , and  $\kappa_\perp = \kappa_\parallel = k_B$  of the local field. In general  $\kappa$  is a parameter determined by local quantities (Medvedev et al. 2005) but is treated as a constant in this paper as it does not significantly alter the shape of the spectrum in the regimes under consideration.

Finally,  $C$  is fixed by the requirement that  $\int K_{\alpha\alpha}(\mathbf{k})d\mathbf{k} = \langle B^2 \rangle$  where  $\langle B^2 \rangle$  is the mean square

value of the local magnetic field. This convention for  $C$  results in a normalization of

$$C = \frac{\langle B^2 \rangle}{\int f_z(k_{\parallel}) k_r f_r(k_r) dk_{\parallel} dk_r} \quad (4)$$

where we have switched from Cartesian to cylindrical coordinates to simplify the integration. Unlike previous works we have chosen to normalize the correlation tensor by the mean square value of the magnetic field in an attempt to directly model the specific magnitudes of the afterglow and prompt emission.

## 2.2 Emission - $j_{\omega}$

We now calculate the emissivity of an ensemble of electrons in the jitter regime. The emissivity of a power-law distributed electrons,  $N \propto \gamma^{-p}$  with a sharp low-energy cutoff  $\gamma \leq \gamma_{\min}$  has been calculated for the simple one-dimensional jitter model in the original paper by Medvedev (2000). In a full three-dimensional treatment of jitter radiation (Medvedev 2006) a single electron spectral power has been calculated. The ensemble emissivity is computed as a convolution of the single electron spectral power with the electron distribution. We present here, for the first time, the total radiation emitted by a distribution of electrons using the coefficients which return the true spectrum as a function of local conditions. Other than the powers on the correlation tensor describing the magnetic field (to which the radiation spectrum is relatively insensitive) every attempt has been made to keep the number of free parameters to a minimum. A general derivation of our work follows.

The formula used to describe the angle averaged radiation emitted by a single, relativistic particle traveling through small scale magnetic fields is given (neglecting plasma dispersion) by

$$\frac{dW}{d\omega} = \frac{e^2 \omega}{2\pi c^3} \int_{\omega/2\gamma^2}^{\infty} \frac{|\mathbf{w}_{\omega'}|^2}{\omega'^2} \left( 1 - \frac{\omega}{\omega' \gamma^2} + \frac{\omega^2}{2\omega'^2 \gamma^4} \right) d\omega', \quad (5)$$

where  $\gamma$  is the Lorentz factor of the particle. Due to approximations used in deriving equation 5 this equation is only valid when the ratio of a particle's angular deflection due to magnetic field fluctuations ( $\alpha$ ) to its relativistic beaming angle ( $\Delta\theta \sim \frac{1}{\gamma}$ ) is much less than one. In keeping with the 2000 paper by Medvedev we define this ratio as

$$\delta \equiv \frac{\gamma}{k_B \rho_e} \sim \frac{\alpha}{\Delta\theta} \quad (6)$$

where  $\rho_e$  is the Larmor radius of an electron. In practice the value of  $\delta$  calculated, using realistic parameters, is quite often  $\ll 1$  and setting it equal to zero in the code has a vanishingly small effect.

The term  $|\mathbf{w}_{\omega'}|^2$  in equation 5 is the square of the Fourier transform of the acceleration field due to the Lorentz forces. Here we replace it with a volume averaged  $\langle |\mathbf{w}_{\omega'}|^2 \rangle$  by assuming a statistically homogeneous turbulence. The derivation of this term is left for the appendix (the interested is referred to Fleishman 2006 for more details) and we state here the result for it by assuming the fields described above

$$\langle |\mathbf{w}_{\omega'}|^2 \rangle = \left( \frac{e}{\gamma m_e} \right)^2 \frac{CT}{2\pi} (1 + \cos^2 \Theta') I(\Theta'), \quad (7)$$

where  $I(\Theta')$  is given by

$$I(\Theta') = \int f_z(k_{\parallel}) f_{xy}(k_{\perp}) \delta(\omega' + \mathbf{k} \cdot \mathbf{v}) d^3 k, \quad (8)$$

where  $\Theta'$  is the angle between a particle's velocity and an observer in the comoving frame,  $C$  is given by equation 4,  $T$  is the period for an electron traveling in Weibel fields, and  $f_z(k_{\parallel})$  and  $f_{xy}(k_{\perp})$  are given by equations 2 and 3 respectively. To evaluate the integral in equation 7 it is necessary to specify both the limits of integration and the geometry of the problem. The limits come from the nature of the magnetic fields generated by the Weibel instability. The Fourier component associated with the fastest growing mode in the Weibel instability is specified by

$$k_{Weibel} = \frac{4\gamma_{shock} \omega_{pe}}{2^{1/4} \bar{\gamma}_e^{1/2} c}. \quad (9)$$

The factor of  $4\gamma_{shock}$  comes from the shock compression and  $\omega_{pe}^2 = \frac{4\pi e^2 n_{Ext}}{m_e}$  is the plasma frequency of the pre-shocked material (which, in the case of afterglows, corresponds to an ISM or wind density profile). While modes will initially be compressed only perpendicular to the shock plane we make the assumption that the spatial scales will be mixed by turbulence and set the inverse length scales,  $k_{\parallel}$ ,  $k_{\perp} = k_{Weibel}$ .

The geometry of the system is defined as follows: The shock is propagating in the  $z$  direction and lies in the  $x$ - $y$  plane. A particle in the shock has a velocity vector given by  $\mathbf{k} = \hat{\mathbf{x}} k \sin \Theta' + \hat{\mathbf{z}} k \cos \Theta'$ , this gives us  $\mathbf{k} \cdot \mathbf{v} = k_x v \sin \Theta' + k_z v \cos \Theta'$ . In his 2006 paper Medvedev choose to present three separate forms for  $\langle |\mathbf{w}_{\omega'}|^2 \rangle$  corresponding to a shock viewed at 0 degrees,  $\pi/2$  and in between these extremes. We have chosen to evaluate equation 8 somewhat differently by using the properties of the delta function to integrate the correlation function in two distinct ways. By doing this we can match the asymptotic forms with two functions as opposed to three and do not suffer from numerical errors that occur when  $\Theta'$  approaches a limit which would introduce infinities. The two forms we use are

$$I_1(\Theta') = \int \frac{1}{|v \cos \Theta'|} f_z \left( \frac{\omega'/v}{\cos \Theta'} + k_x \tan \Theta' \right) f_{xy}(k_x) dk_x, \quad (10)$$

and

$$I_2(\Theta') = \int \frac{1}{|v \sin \Theta'|} f_z(k_z) f_{xy} \left( \frac{\omega'/v}{\sin \Theta'} + \frac{k_z}{\tan \Theta'} \right) dk_z, \quad (11)$$

where the bar in  $f_{xy}$  denotes an integration over  $k_y$ . In Fourier space the modes which generate fields lie within a spherical annulus with radius  $k_{\perp}$  and  $k_{\parallel} \in [\delta k_{Weibel}, k_{Weibel}]$  and this sets the limits for the integrals in equations 10 and 11. Physical distances greater than  $\sim \frac{1}{\delta k_{Weibel}}$  do not generate fields and as such do not contribute to the emergent spectrum. Choosing  $v \sim c$  and switching between forms for  $\Theta' \sim \frac{\pi}{4}$  we are able to reproduce the results of Medvedev (2006). Combining equations (2), (3), (4), (5), (7), (10), and (11) and multiplying the result by  $\frac{1}{T}$  gives us

$$P(\omega) = \frac{1}{T} \frac{dW}{d\omega} \quad (12)$$

the total energy per unit frequency, per unit time, emitted by a single electron in Weibel generated fields. Unlike the case of synchrotron, where it is possible to precisely define an orbital

period, the random, small scale nature of Weibel turbulence requires a more arbitrary choice so we choose to use the form adopted by Medvedev (2006) and Fleishman (2006) which includes the value for the period in the magnetic field derivation (see equation 7. By using this method  $T$  simply disappears from the final form for  $P(\omega)$ .

The final step required to calculate the emission from a population of electrons is to choose the form for the distribution. It is standard to assume that the electrons follow a power law distribution

$$n'(\gamma) = K\gamma^{-p} \quad (13)$$

where  $\gamma \in [\gamma_{min}, \infty]$ ,  $K = (p-1)n'\gamma_{min}^{p-1}$  and  $\gamma_{min} = \frac{p-2}{p-1} \frac{\epsilon_e e'}{n' m_e c^2}$  in which the primed quantities  $n'$  and  $e'$  refer to the comoving number and energy densities and  $\epsilon_e$  is the fraction of the thermal energy in the electrons.

Combining equations 13 and 12 and integrating from  $\gamma_{min}$  to  $\infty$  yields the final result

$$P_{tot}(\omega) = \int_{\gamma_{min}}^{\infty} n'(\gamma) P(\omega) d\gamma. \quad (14)$$

It is this equation which we have numerically solved for any value of  $\Theta'$ . To arrive at the final form for  $j_\omega$  we assume a random distribution of emitting particles and divide 14 by  $4\pi$ .

To confirm our results we have done the following: First is possible to analytically show (for  $\beta_{1,2} = 0$ ) that combining the  $\Theta' = 0$  form of  $\langle |\mathbf{w}_\omega|^2 \rangle$  with equation 4.92 ( $2e^2\gamma^4/3c^3$ )( $w_\perp^2 + \gamma^2 w_\parallel^2$ ) of Rybicki & Lightman (1979) which describes the instantaneous power emitted by a single relativistic electron reduces to

$$dW/dt = (2/3)r_e^2 c \gamma^2 \langle B^2 \rangle, \quad (15)$$

which is equivalent to the case of synchrotron radiation. We have confirmed that our procedure numerically returns the same value by integrating equation 5. Setting  $\beta_{1,2} \neq 0$  in our code does not change this result. Our second confirmation of code was done by replacing  $P(\omega)$  in equation (14) with the the form for synchrotron and verifying that our technique yielded results which were in agreement with the analytic form for  $P_{tot, Synch}(\omega)$  given by equation 6.36 in (Rybicki & Lightman 1979).

### 2.3 Absorption - $\alpha_\omega$

Given the single particle emissivity,  $P(\nu)$ , and the particle energy distribution, calculation of the jitter self-absorption is straightforward. We have analytically calculated it (Medvedev, et al. 2007) in the regimes when the self-absorption frequency is above and below the jitter peak frequency. For numerical implementation, the self-absorption coefficient can be derived  $\alpha_\omega$  using equation 6.50 from Rybicki & Lightman (1979) as follows:

$$\alpha_\nu = -\frac{c^2}{8\pi\nu^2} \int P(\nu, E) E^2 \frac{\partial}{\partial E} \left[ \frac{N(E)}{E^2} \right] dE \quad (16)$$

Using  $P(\nu, E) = 2\pi P(\omega)$ ,  $E = \gamma m_e c^2$ ,  $N(E) = \frac{d\gamma}{dE} n(\gamma)$ , and  $\omega = 2\pi\nu$  where  $n(\gamma)$  and  $p(\omega)$  are given by equations 12 and 13, quickly yields

$$\alpha_\omega = \frac{(p+2)\pi^2 k}{m_e \omega^2} \int_{\gamma_{min}}^{\infty} \gamma^{-(p+1)} P(\omega) d\gamma. \quad (17)$$

Effectively, once the numerical problem of solving equation 14 has been solved the only modification necessary to solve for the absorption coefficient is a change in the power on gamma and a change in the normalization constant.

## 3 RESULTS

To get an idea of the results, we can set up a test case of a single internal shock within the prompt burst. The material has a preshock density of  $9.25 \times 10^{-12}$  g/cm<sup>3</sup>, a shock Lorentz factor of  $\gamma_{int} = 2$ ,  $\epsilon_e = 0.2$ , and a magnetic equipartition fraction  $\epsilon_B = 10^{-5}$ . The thickness of the shell is  $3 \times 10^7$  cm in the observer's frame and the material is moving with a bulk Lorentz factor of 100. We consider a shell radiating at  $R = 10^{14}$  cm. This setup corresponds to an isotropic energy of  $5 \times 10^{51}$  ergs in the shell. These values are chosen to give a peak frequency of about 200 KeV in the observer's frame. We have chosen the parameters describing magnetic field distribution, namely  $\alpha_{1,2} > 0.5$  and  $\beta_{1,2} > \alpha_{1,2} + p/2$ , so that they do not affect spectral characteristics. It is important to keep in mind that the emission angles correspond to the co-moving angles. The results plotted are the observed quantities as a function of co-moving emission angle.

Figure 1 shows emissivity vs. frequency for different emission angles. For  $\theta' = 0$  the emission has a slope of 1 at low frequencies and then turns over to a slope of  $-0.75$ , set by the electron power index. As angle increases, the low frequency slope near the peak decreases, and at much lower frequencies the slope flattens to 0. Beyond an angle of  $30^\circ$ , there is no longer a peak in the spectrum, just a transition from a constant value (slope 0) to a slope of  $-0.75$ . The value of the low frequency constant changes with angle, peaking at  $45^\circ$  and then decreasing. At high frequencies, the slope is always the same but the emissivity at a given frequency decreases with angle. These results are in full agreement with the single electron spectra of Medvedev (2006).

Figure 2 shows the absorption coefficient  $\alpha$  for the same setup. The absorption coefficient is proportional to  $P(\omega) \times \omega^2$  below the peak frequency and to  $P(\omega) \times \omega^{2.5}$  above the peak frequency.

With  $P(\omega)$  and  $\alpha$  we can solve the 1D radiative transfer equation to find the specific intensity of the shell at different angles. Assuming the observable portion of the shell is spherical and that the amount of time any piece of the shell is radiating is short compared to the time it takes the shell to become visible (i.e., we assume the shell is infinitely thin), the specific intensity at a given angle will be proportional to the total emission at the time that angle comes into view. Figure 3 shows the integrated specific intensity at different angles for jitter radiation. Figure 4 shows synchrotron radiation for identical conditions and angles.

The synchrotron radiation spectrum shows no change in the shape of the spectrum. The peak frequency decreases by about a factor of 2 and the power decreases by a factor  $\sim 7$  between  $0^\circ$  and  $90^\circ$  due to relativistic effects. Jitter radiation, on the other hand, shows a large change in spectral index and total emission below the peak frequency and a decrease in emission of about a factor of 12 with angle above the peak frequency. Note that the source function for jitter and synchrotron are the same for identical conditions. Self absorption becomes important at a few eV in this example.

The time at which different angles come into view is found from the geometric time delay to be  $(1 - \cos \theta) \times r/c$  where  $\theta$  is the emission angle in the observer's frame,  $r$  is the emission radius ( $10^{14}$  cm in this example) and  $c$  is the speed of light.

Figure 5 shows intrinsic brightness vs. time at 10, 100, and 1000 KeV and 1 eV (1240 nm). At 1000 KeV, above the initial peak frequency, emission decreases with time by a factor of about 12. At 100 KeV, just below the initial peak frequency, emission increases slightly for 0.01 s and then decreases. At 10 KeV emission increases by a factor of 10 in 0.03 s, corresponding to  $40^\circ$ , and then decreases. The initial amount of increase is larger at lower energies. At 1 eV, there is an initial increase but then the emission becomes optically thick and nearly constant with time. This has important implications for the interpretation of spectral lags and the optical emission during the prompt phase. As is clear from Fig. 5, the optical and high energy bands can show very little correlation, even if they come from the same electrons and the same emission mechanism. Lack of correlation was used as an argument in favor of a reverse shock origin of the optical flash in GRB 990123 (Akerlof et al. 1999, Sari et al. 1999). The flattening of the spectra in the X-ray band could also explain the soft X-ray excesses detected in some events (Preece et al. 1996; Strohmayer et al. 1998).

Figures 6 shows the ratio of the total number of photons between 110 and 320 KeV to the number of photons between 55 and 110 KeV vs. time. This ratio is equivalent to the count ratio of BATSE channels 3:2 ( $HR_{3/2}$ ). This plot shows a hard to soft evolution for the first 0.03 s (out to a  $40^\circ$  angle) and then a fairly flat hardness ratio after this.

Let us now consider the external shock phase. For an example comparison of the afterglow spectrum for jitter and synchrotron radiation we examine an isotropic explosion with an energy of  $10^{53}$  ergs expanding into a medium with a density of 1 particle/cm<sup>3</sup> at the observed time  $t = 1000$  s. The Blandford-McKee (Blandford & McKee, 1976) solution for a relativistic fireball is used to determine the density, internal energy and Lorentz factor for material at the leading edge of the shock. A magnetic field energy of  $\epsilon_B = 10^{-4}$  of equipartition and  $\epsilon_e = 0.01$  are assumed everywhere, and a shock thickness of  $\frac{r}{2\gamma^2} \approx 2.4 \times 10^{14}$  cm everywhere is assumed. Figure 7 shows a comparison between the emission from jitter and synchrotron radiation under these conditions. Both spectra peak at about 0.1 eV, but relative location of the peak frequencies is dependent on the particular parameters used. Below the peak frequency, the synchrotron emission increases with frequency as  $\nu^{1/3}$ , while the jitter spectrum is nearly flat. This is because large angles dominate the afterglow spectrum (see also Medvedev, et al., 2007). The synchrotron and jitter spectra become optically thick at around  $10^{-5}$  eV (2.4 GHz) and  $10^{-4}$  eV (24 GHz), respectively, in this example, but this is dependent on the thickness of the afterglow material.

## 4 SUMMARY AND DISCUSSION

We have computed jitter radiation spectra for a non-thermal population of relativistic electrons radiating in a highly non-uniform magnetic field, including self absorption. Our results are in full agreement, when relevant, with previous compu-

tations (Medvedev 2006; Medvedev, et al., 2007). We find that depending on the orientation of the line of sight with respect to the shock front the jitter spectrum is different. For head on shocks, the spectrum is peaked, with a steep low energy slope  $F(\nu) \propto \nu$ . For edge on shocks, the spectrum at the left of the peak is flat down to the self absorption frequency. We applied these results to standard GRB cases, for the prompt and for the afterglow emission. We find that, in addition to some of the observations already discussed in the previous literature (Medvedev 2000, 2006), jitter radiation can explain X-ray excesses in the prompt spectrum and the lack of correlation between optical and high energy radiation. This is due to the fact that the optical radiation lies in the regime where the spectral slope depends on the orientation angle, while the high energy emission depends only on parameters that do not evolve with time. We also find that jitter radiation explains naturally the presence of spectral lags (Norris et al. 2001).

In the afterglow regime, the optical and X-ray spectra are very similar to those of synchrotron radiation. At frequencies below the peak one, differences are instead clearly visible. First, the spectrum is flat ( $F(\nu) \propto \nu^0$  instead of  $F(\nu) \propto \nu^{1/3}$ ); second, the self absorption frequency is at higher frequencies (see also Medvedev, et al. (2007) who also show that self absorption frequency has a different temporal evolution in jitter and synchrotron). Understanding the implications of those differences is not simple and a proper fit has to be performed (Morsony et al. in preparation). It is likely that jitter spectra fit to afterglow data will give different results in term of the properties of the ambient medium, since radio observations are always very important in constraining the density of the interstellar material. A more detailed discussions will be possible only after formal fit have been performed.

## ACKNOWLEDGEMENTS

This work was supported by NSF grants AST-0407040 (JW) and AST-0307502 (BM, DL), NASA Astrophysical Theory Grants NNG04GL01G and NNX07AH08G (JW), NNG06GI06G (BM, DL) and NNG-04GM41G (MM), Swift Guest Investigator Program grants NNX06AB69G (BM, DL) and 06-SWIFT306-0001 (MM), and DoE grant DE-FG02-04ER54790 (MM). MM gratefully acknowledges support from the Institute for Advanced Study.

## REFERENCES

- Akerlof C., et al., 1999, *Nature*, 398, 400
- Blandford, R. D., & McKee, C. F. 1976, *Physics of Fluids*, 19, 1130
- Covino S., et al., 1999, *A&A*, 348, L1
- Crider A., et al., 1997, *ApJ*, 479, L39
- Fleishman, G. 2006, *ApJ*, 638, 348
- Frederiksen, J., Hededal, C., Haugbølle, T. & Nordlund, Å., 2004, *ApJ*, 608, L13
- Ghisellini G., Celotti A., Lazzati D., 2000, *MNRAS*, 313, L1
- Granot, J., Piran, T., & Sari, R. 1999, *ApJ*, 513, 679
- Granot, J., Piran, T., & Sari, R. 1999, *ApJ*, 527, 236
- Gruzinov A., 2001, *ApJ*, 563, L15
- Landau, L. D., & Lifshitz, E.M. 1971, *The Classical Theory of Fields* (Oxford: Pergamon Press)

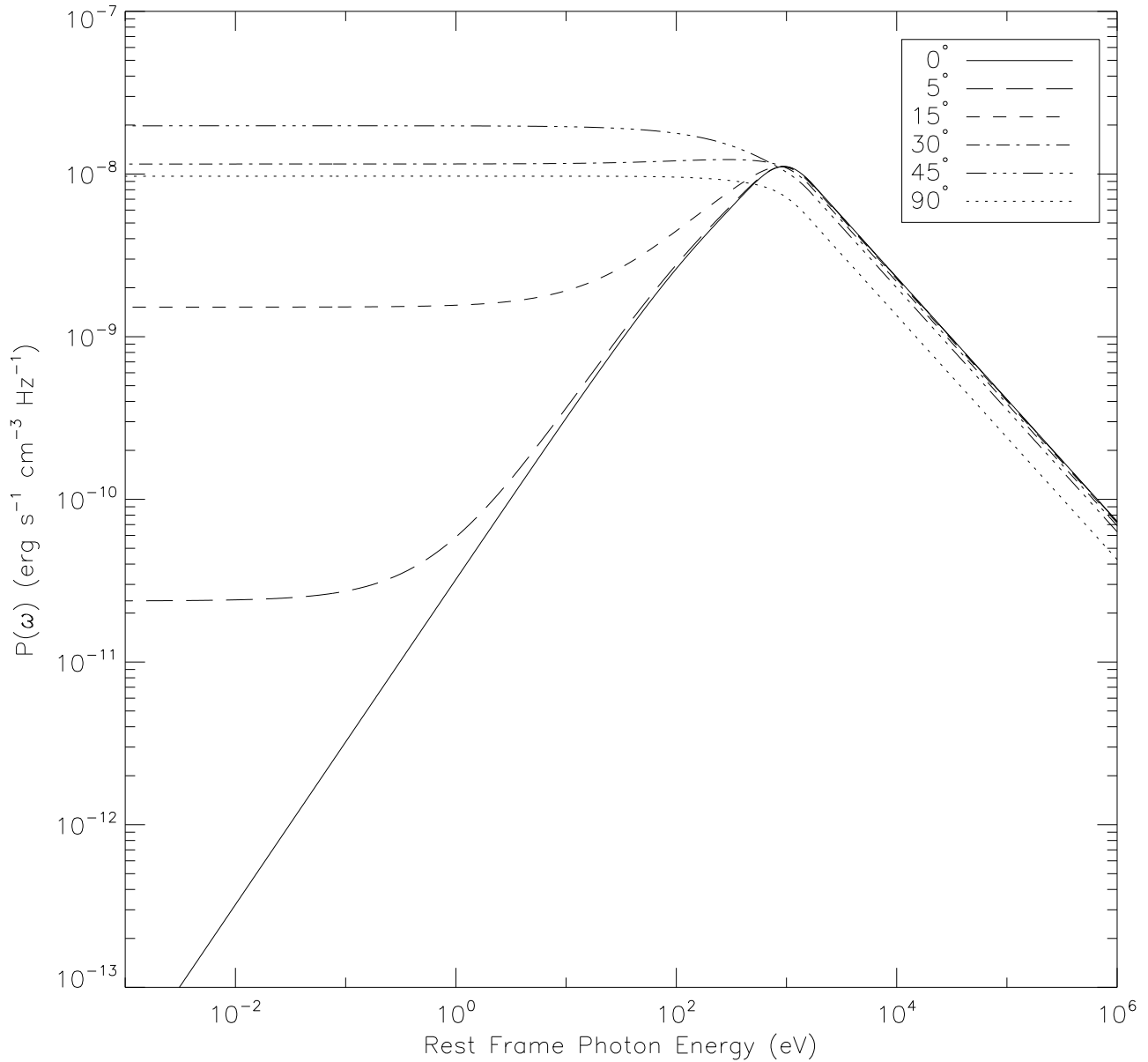


**Figure 1.** Emissivity vs. frequency at different angles. Angles plotted are  $\theta' = 0^\circ$  (solid line),  $5^\circ$  (long-dashed line),  $15^\circ$  (dashed line),  $30^\circ$  (dot-dash line),  $45^\circ$  (3 dot-dash), and  $90^\circ$  (dotted line).

Lazzati D., et al., 2004, *A&A*, 422, 121  
 Medvedev, M. V. 2000, *ApJ*, 540, 704  
 Medvedev, M. V. 2006, *ApJ*, 637, 869  
 Medvedev, M. V., & Loeb, A. 1999, *ApJ*, 526, 697  
 Medvedev, M. V., Fiore, M., Fonseca, R., Silva, L. O., & Mori, W. 2005, *ApJ*, 618, L75  
 Medvedev, M. V., Lazzati, D., Morsony, B. C., & Workman, J. C., 2007, *astro-ph/0703209*  
 Meszaros P., Rees M. J., 1997, *ApJ*, 476, 232  
 Nishikawa, K.-I., Hardee, P., Richardson, G., Preece, R., Sol, H., & Fishman, G. J. 2003, *ApJ*, 595, 55  
 Panaitescu A., Kumar P., 2001, *ApJ*, 554, 667  
 Piran T., 1999, *PhR*, 314, 575  
 Piran, T. 1999, *Physics Reports*, Volume 314, Issue 6, 575  
 Preece R. D., Briggs M. S., Pendleton G. N., Paciesas W. S.,

Matteson J. L., Band D. L., Skelton R. T., Meegan C. A., 1996, *ApJ*, 473, 310  
 Preece R. D., Briggs M. S., Mallozzi R. S., Pendleton G. N., Paciesas W. S., Band D. L., 1998, *ApJ*, 506, L23  
 Rybicki, G. B., & Lightman, A. P. 1979, *Radiative Processes in Astrophysics*, (New York: Wiley)  
 Sari R., Piran T., Halpern J. P., 1999, *ApJ*, 519, L17  
 Silva, L. O., Fonseca, R. A., Tonge, J. W., Dawson, J. M., Mori, W. B., & Medvedev, M. V. 2003, *ApJL*, 596, L121  
 Strohmayer T. E., Fenimore E. E., Murakami T., Yoshida A., 1998, *ApJ*, 500, 873  
 Weibel, E. S. 1959, *Phys. Rev. Lett.*, 2, 83  
 Wijers R. A. M. J., Galama T. J., 1999, *ApJ*, 523, 177  
 Zhang, B. & Mészáros 2004, *International Journal of Modern Physics*, 19, 2385

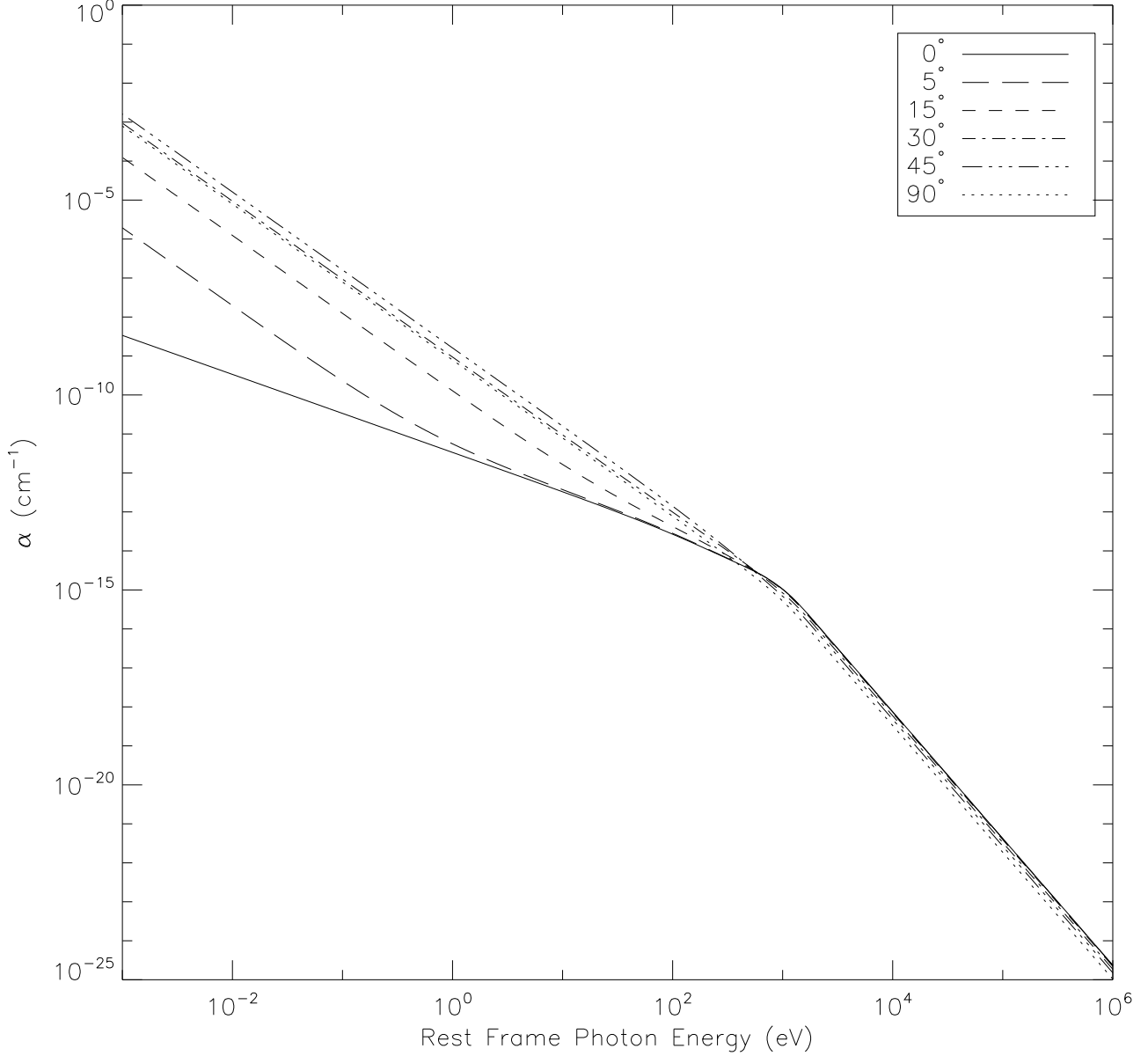


**Figure 2.** Absorption coefficient  $\alpha$  vs. frequency at different angles. Angles plotted are  $\theta' = 0^\circ$  (solid line),  $5^\circ$  (long-dashed line),  $15^\circ$  (dashed line),  $30^\circ$  (dot-dash line),  $45^\circ$  (3 dot-dash), and  $90^\circ$  (dotted line).

#### APPENDIX A: DERIVATION OF $\langle |\mathbf{W}_{\omega'}|^2 \rangle$

The following derivation is taken from Medvedev (2006) and Fleishman (2006). First, let us define a parameter  $\delta$  which defines the ratio of deflection ( $\alpha$ ) due to Lorentz forces and beaming ( $\Delta\theta$ ) due to relativistic effects experienced by a particle moving with Lorentz factor  $\gamma$  in a small scale, random magnetic field with a typical correlation length,  $k_B$  and Larmor Radius,  $\rho_e$ .

$$\delta \equiv \frac{\gamma}{k_B \rho_e} \sim \frac{\alpha}{\Delta\theta} \quad (\text{A1})$$

For values of  $\delta \ll 1$  the particle trajectory is nearly a straight line (with small perpendicular motions introduced by the Lorentz forces). In this case the angle averaged spectral en-

ergy, neglecting plasma dispersion, is given by Landau & Lifshitz (1971)

$$\frac{dW}{d\omega} = \frac{e^2 \omega}{2\pi c^3} \int_{\omega/2\gamma^2}^{\infty} \frac{|\mathbf{w}_{\omega'}|^2}{\omega'^2} \left( 1 - \frac{\omega}{\omega' \gamma^2} + \frac{\omega^2}{2\omega'^2 \gamma^4} \right) d\omega' \quad (\text{A2})$$

where  $\mathbf{w}_{\omega'}$  is the Fourier transform of the transverse acceleration of the particle due to Lorentz forces ( $\mathbf{w} \equiv F_L/\gamma m$ ). Fourier transforming the acceleration field along a particles trajectory  $\mathbf{w}(\mathbf{r}_0 + \mathbf{v}t, t)$  yields

$$\mathbf{w}_{\omega'} = (2\pi)^{-4} \int e^{i\omega' t} dt \left( e^{-i(\Omega t - \mathbf{k} \cdot \mathbf{r}_0 - \mathbf{k} \cdot \mathbf{v}t)} \mathbf{w}_{\Omega, \mathbf{k}} d\Omega d\mathbf{k} \right)$$

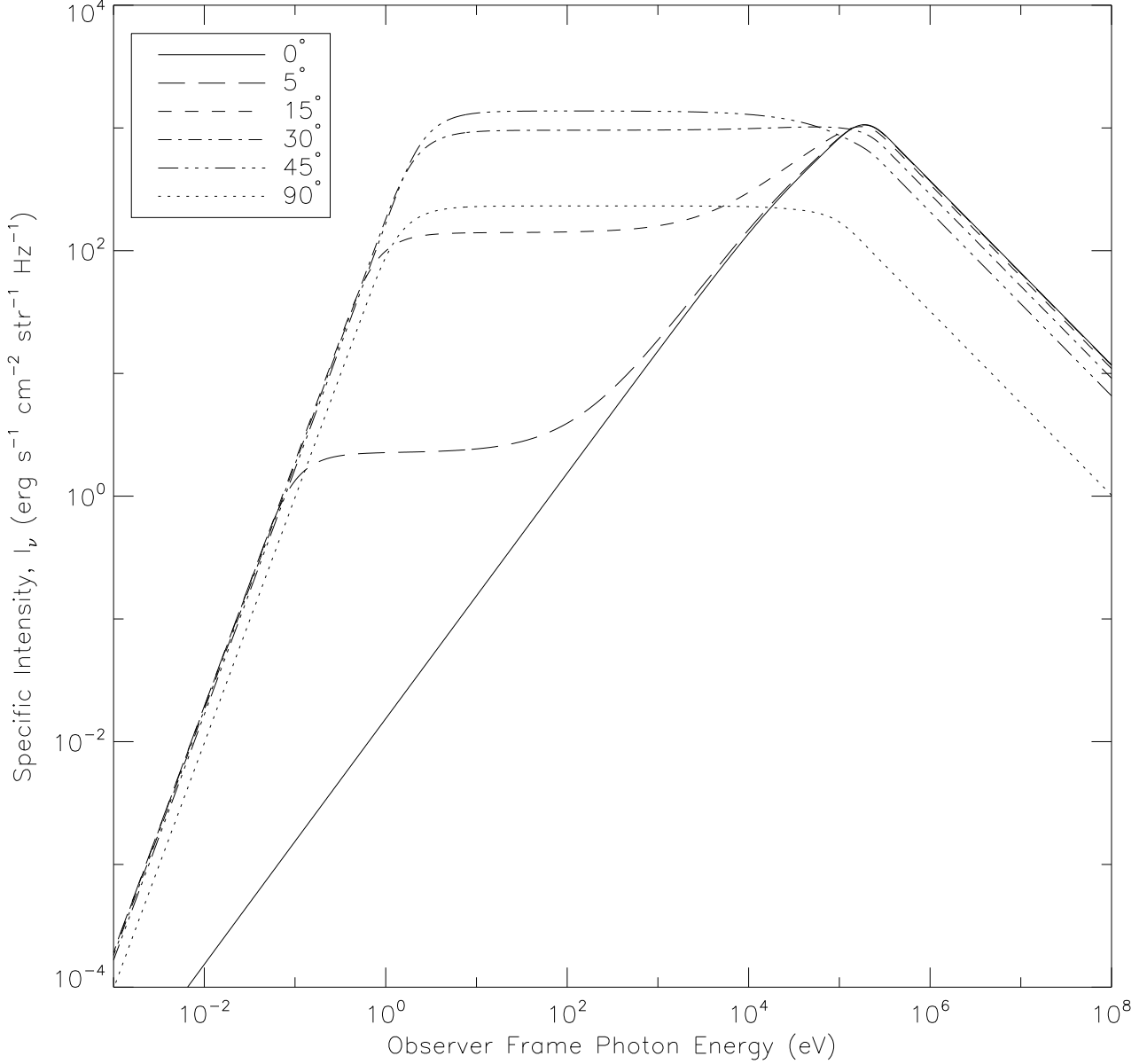


**Figure 3.** Jitter emission for a single relativistic shell at different angles. Angles plotted are  $\theta' = 0^\circ$  (solid line),  $5^\circ$  (long-dashed line),  $15^\circ$  (dashed line),  $30^\circ$  (dot-dash line),  $45^\circ$  (3 dot-dash), and  $90^\circ$  (dotted line). Jitter radiation peaks at about 190 KeV.

$$= (2\pi)^{-3} \int \mathbf{w}_{\Omega, \mathbf{k}} \delta(\omega' - \Omega + \mathbf{k} \cdot \mathbf{v}) e^{i\mathbf{k} \cdot \mathbf{r}_0} d\Omega d\mathbf{k}. \quad (\text{A3})$$

Squaring the above result and averaging over volume using the results  $\langle |\mathbf{w}_{\omega'}|^2 \rangle = V^{-1} \int |\mathbf{w}_{\omega'}|^2 d\mathbf{r}_0$  and  $\int e^{i(\mathbf{k}-\mathbf{k}_1) \cdot \mathbf{r}_0} d\mathbf{r}_0 = (2\pi)^3 \delta(\mathbf{k} - \mathbf{k}_1)$  yields

$$\langle |\mathbf{w}_{\omega'}|^2 \rangle = (2\pi)^{-3} V^{-1} \int |\mathbf{w}_{\Omega, \mathbf{k}}|^2 \delta(\omega' - \Omega + \mathbf{k} \cdot \mathbf{v}) d\Omega d\mathbf{k}. \quad (\text{A4})$$

In the absence of electric fields the Lorentz acceleration is given by  $(e/\gamma mc)\mathbf{v} \times \mathbf{B}$  which, in tensor notation, is  $(e/\gamma mc)\frac{1}{2}e_{\alpha\beta\gamma}(v_\beta B_\gamma - v_\gamma B_\beta)$ . After simplification this expression results in

$$|\mathbf{w}_{\Omega, \mathbf{k}}|^2 = (ev/\gamma mc)^2 (\delta_{\alpha\beta} - v^{-2} v_\alpha v_\beta) B_{\Omega, \mathbf{k}}^\alpha B_{\Omega, \mathbf{k}}^{*\beta}. \quad (\text{A5})$$

where  $B_{\Omega, \mathbf{k}}^\alpha B_{\Omega, \mathbf{k}}^{*\beta}$  is the Fourier Transform of the field correlation tensor

$$B_{\Omega, \mathbf{k}}^\alpha B_{\Omega, \mathbf{k}}^{*\beta} = TV K_{\alpha\beta}(\Omega, \mathbf{k}) = TV \int e^{i(\Omega t - \mathbf{k} \cdot \mathbf{r})} K_{\alpha\beta}(\mathbf{r}, t) d\mathbf{r} dt, \quad (\text{A6})$$

where T can be interpreted as the period or duration of emission, V is the volume integrated over and  $K_{\alpha\beta}(\mathbf{r}, t)$  is the second order correlation tensor of the magnetic field. Using the results above and assuming a time independent magnetic field, equations (A4), (A5) reduce to

$$\langle |\mathbf{w}_{\omega'}|^2 \rangle = (2\pi V)^{-1} \int |\mathbf{w}_{\mathbf{k}}|^2 \delta(\omega' + \mathbf{k} \cdot \mathbf{v}) d\mathbf{k}, \quad (\text{A7})$$

$$|\mathbf{w}_{\mathbf{k}}|^2 = (ev/\gamma mc)^2 (\delta_{\alpha\beta} - v^{-2} v_\alpha v_\beta) V T K_{\alpha\beta}(\mathbf{k}). \quad (\text{A8})$$



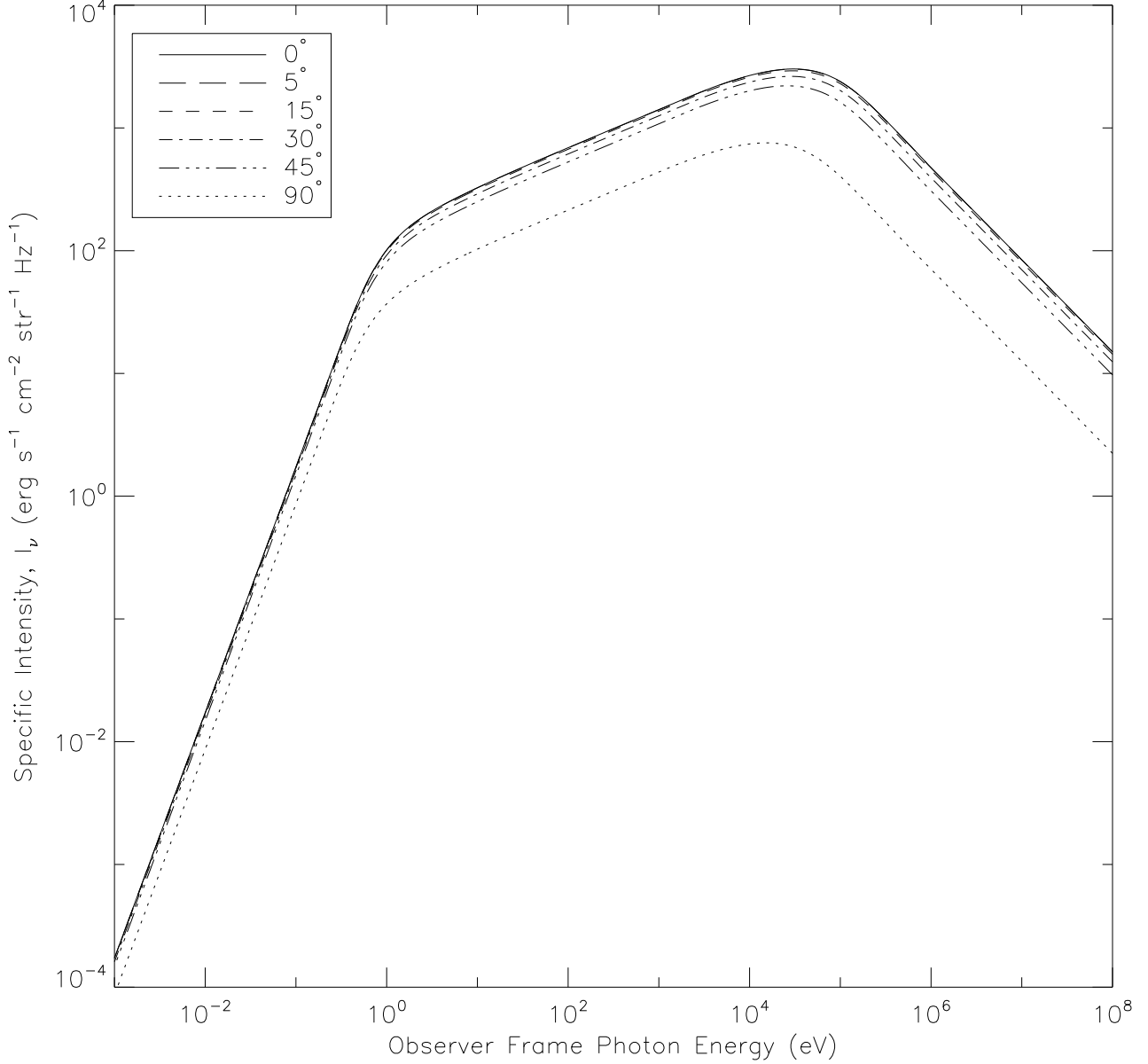


**Figure 4.** Synchrotron emission for a single relativistic shell at different angles. Angles plotted are  $\theta' = 0^\circ$  (solid line),  $5^\circ$  (long-dashed line),  $15^\circ$  (dashed line),  $30^\circ$  (dot-dash line),  $45^\circ$  (3 dot-dash), and  $90^\circ$  (dotted line). Synchrotron radiation peaks at about 1 MeV

The form of  $K_{\alpha\beta}(\mathbf{k})$  used in this paper is taken from numerical simulations of the Weibel Instability and is given by

$$K_{\alpha\beta}(\mathbf{k}) = C(\delta_{\alpha\beta} - n_\alpha n_\beta) f_z(k_\parallel) f_{xy}(k_\perp), \quad (\text{A9})$$

where  $\mathbf{n}$  is the normal to the shock front,  $C$  is proportional to the mean square magnetic field  $\langle B^2 \rangle$ , and  $f_z(k_\parallel)$  and  $f_{xy}(k_\perp)$  describe the structure of the magnetic field parallel and perpendicular to the shocks normal. Inserting the above into equations (A4), (A5) and simplifying  $(\delta_{\alpha\beta} - v_\alpha v_\beta / v^2)(\delta_{\alpha\beta} - n_\alpha n_\beta) = 1 + (n_\alpha v_\alpha)^2 / v^2 = 1 + \cos^2 \Theta'$ , finally gives the result (for  $v \sim c$ ; Medvedev 2006)

$$\langle |\mathbf{w}_{\omega'}|^2 \rangle = \left( \frac{e}{\gamma m} \right)^2 \frac{CT}{2\pi} (1 + \cos^2 \Theta') \times$$

$$\times \int f_z(k_\parallel) f_{xy}(k_\perp) \delta(\omega' + \mathbf{k} \cdot \mathbf{v}) dk_\parallel d^2 k_\perp. \quad (\text{A10})$$

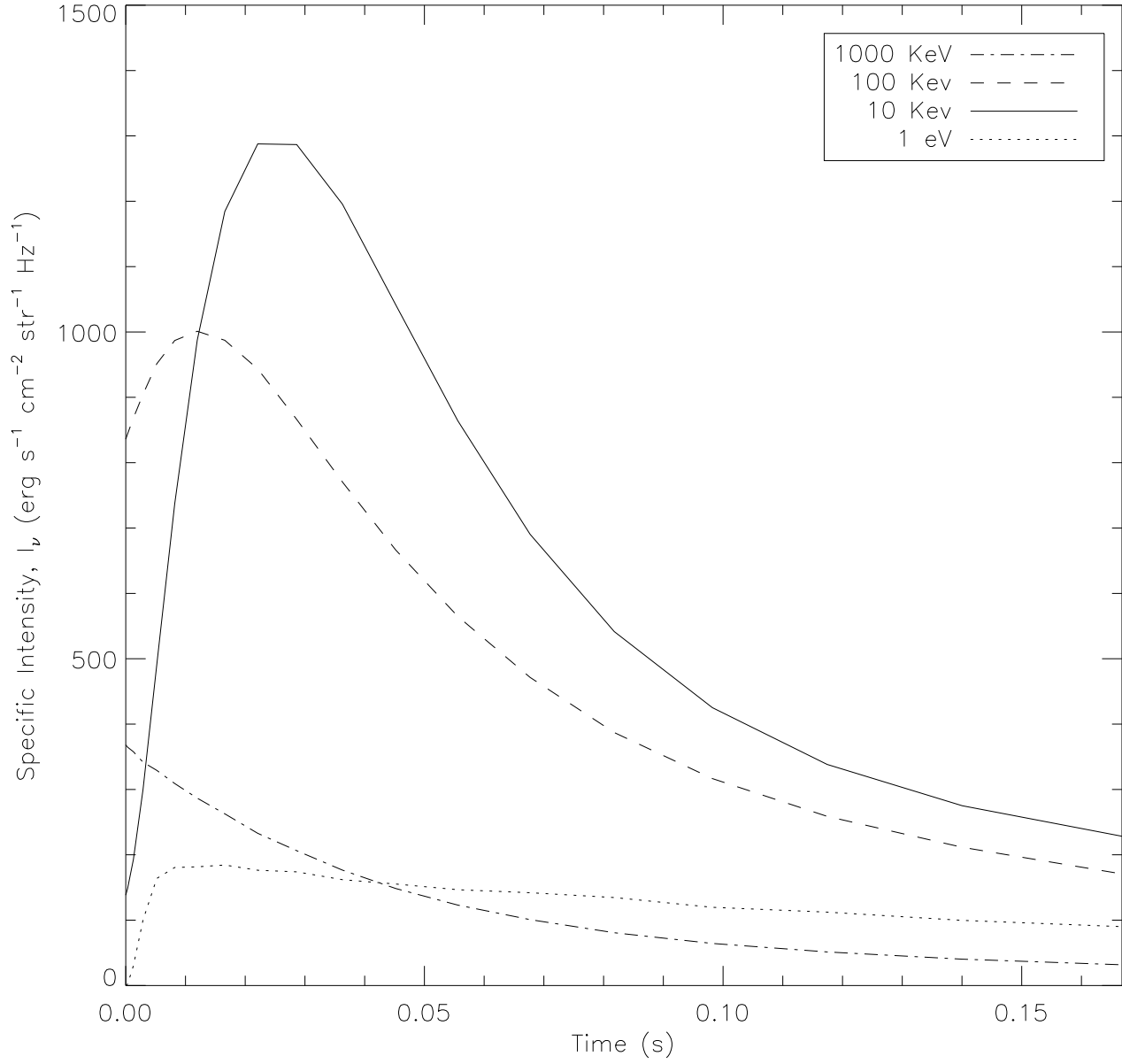


**Figure 5.** Jitter radiation emission vs. time for 1000 KeV (dot-dash line), 100 KeV (dashed line), 10 KeV (solid line) and 1 eV (dotted line). Above the peak emission energy, emitted power decreases with by about 50% while at lower energies the emission increases for 0.1 s and then decreases.

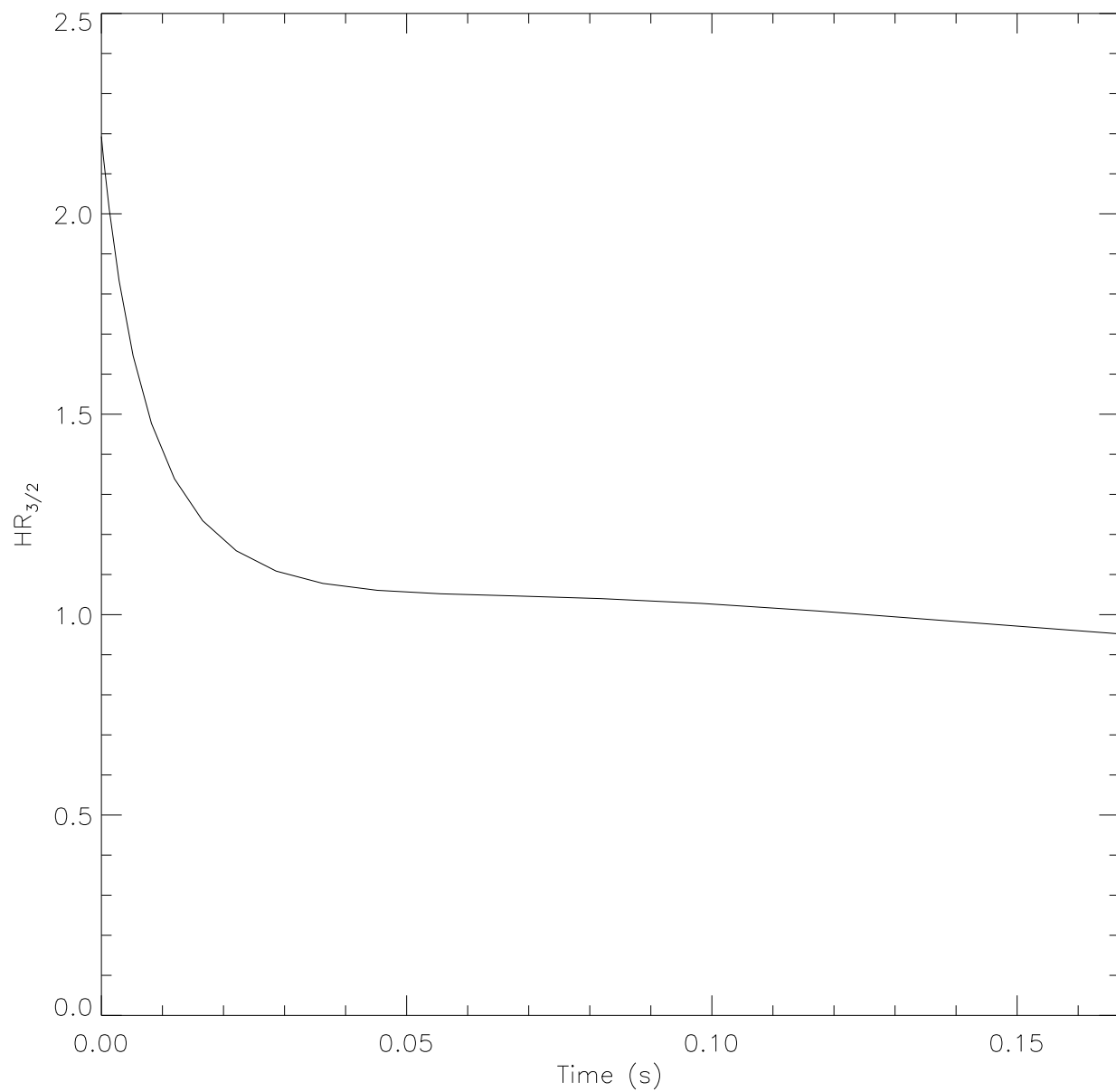


**Figure 6.** Simulated BASTE 3:2 hardness ratio vs. time.  $HR_{3/2}$  is defined as the ratio of the number of photons between 110 KeV and 320 KeV to the number of photons between 55 KeV and 110 KeV.

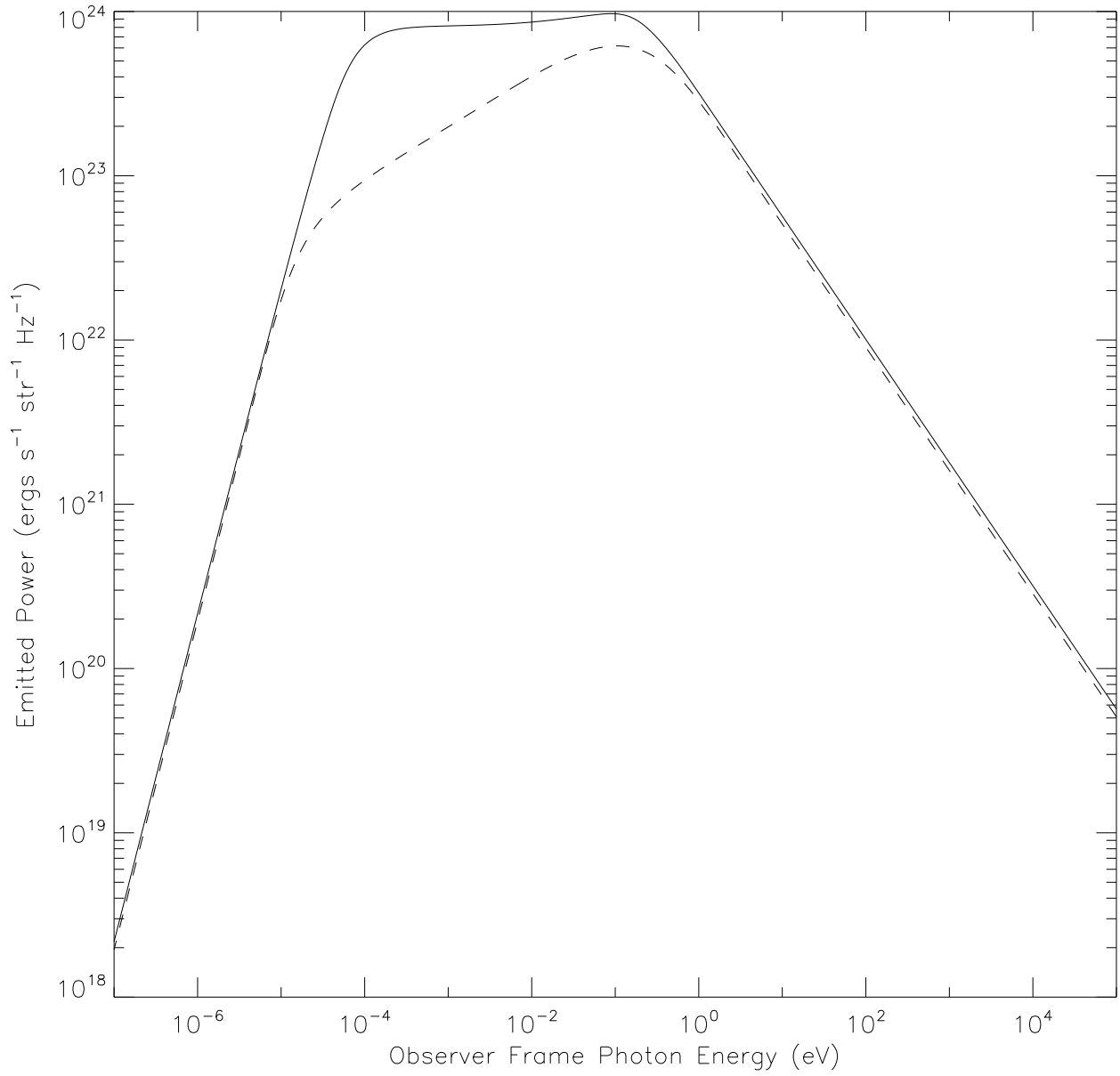


**Figure 7.** Total afterglow power emitted at 1000 s for jitter (solid line) and synchrotron (dashed line) radiation mechanisms under identical conditions.